Eur. Phys. J. A **12**, 191–197 (2001)

THE EUROPEAN PHYSICAL JOURNAL A

© Società Italiana di Fisica
Springer-Verlag 2001

Study of deuteron breakup in light targets at intermediate energies

Yu.L. Parfenova[1,2,a] and M.V. Zhukov[2]

[1] Institute of Nuclear Physics, Moscow State University, 119899 Moscow, Russia
[2] Department of Physics, Chalmers University of Technology and Göteborg University, S-41296 Göteborg, Sweden

Received: 30 May 2001 / Revised version: 2 October 2001
Communicated by M. Garçon

Abstract. Reaction cross-sections and proton removal cross-sections in deuteron-induced reactions with carbon and beryllium targets are studied at intermediate energies. The cross-sections calculated in eikonal approximation show a good agreement with experimental data. The sensitivity of the cross-sections to the target structure, the nucleon-target interaction potential, and the spatial distribution of nucleons in the deuteron is discussed.

PACS. 25.45.-z ^{2}H-induced reactions – 25.60.Dz Interaction and reaction cross-sections

1 Introduction

In the last decades exotic (halo) nuclei have been objects of intensive experimental and theoretical studies. Most of the information is obtained in reactions at intermediate and high energies (above 30 MeV/nucleon), in particular, in the breakup reactions. Many of these reactions have been studied [1–6] in the interactions with light targets where the role of the Coulomb breakup is small.

Theoretical analysis of the projectile breakup at intermediate and high energies is commonly carried out in the eikonal approximation of the Glauber model [5,7–9]. Since the eikonal approximation is widely used for the study of exotic (halo) nuclei [3–5] it seems very important to test the accuracy of this model on the well-known nuclei with a small binding energy and halo-like structure. From this point of view, the deuteron-nucleus interaction is of great interest. Because of its small breakup energy and the dominance of the s-wave in the ground state, the deuteron can be considered as the simplest example of a halo nucleus. Of particular interest are the deuteron breakup processes induced by the strong interactions with target, such as the deuteron dissociation in the nuclear field and the nucleon stripping [10].

The Glauber model [8,11–13] has been already applied to deuteron reactions (breakup, inclusive and exclusive stripping, etc., see for example refs. [10,14–16]). The present work is motivated by new experimental data for the deuteron breakup on a ^{9}Be target in a wide deuteron energy range [17].

In addition to these experimental data, there is an experimental information on the deuteron-nucleus cross-sections. In particular, the deuteron reaction cross-sections σ_R^D are systematically measured for a carbon target [18–23] and there are few measurements for a beryllium target [19,20].

The reaction cross-sections of the deuteron fragments (a proton and a neutron) with different targets are well known and available for different targets in a wide energy range. Different systematics of the parameters of the nucleon-target interaction potentials are developed now (see, for example [24–27]).

All the above-mentioned experimental information can provide different tests of the accuracy of the eikonal approximation in the calculations of deuteron-induced reactions. For example, there is a relation between the nucleon removal cross-sections and reaction cross-sections in the eikonal approximation. In the case of the deuteron-induced reactions, the proton removal cross-section, σ_{-p} is expressed through the neutron reaction cross-section σ_R^n and deuteron reaction cross-section σ_R^D as

$$\sigma_{-p} = \sigma_R^D - \sigma_R^n. \quad (1)$$

Thus, using the available experimental data for the deuteron reaction cross-sections σ_R^D, neutron reaction cross-sections σ_R^n, and nucleon removal cross-sections, σ_{-n}, measured independently, the validity of the eikonal approximation for the calculations of the cross-sections can be tested.

The test of the validity of the relation (1) is important, especially in the analysis of the one-nucleon removal in the halo-nucleus–induced reactions, where the experi-

[a] e-mail: parfenov@fy.chalmers.se

mental information on the cross-sections is often not complete.

To obtain the breakup of the deuteron on light target in the eikonal approximation, we will use realistic nucleon-target interaction potentials and realistic density distributions of the target nucleus. The density distributions are fitted to reproduce the r.m.s. charge radii of nuclei. We also use the realistic wave function (WF) of the neutron-proton relative motion in the deuteron. The realistic WF is obtained as a solution of the Schrödinger equation, reduced to the set of coupled linear differential equations with a realistic potential. The ground state of the deuteron is represented by 93.6% of s-wave and 6.4% d-wave.

In our calculations, the Coulomb dissociation is not considered. It is shown in refs. [14,28] that its contribution to the reaction cross-sections for ^{9}Be and ^{12}C targets is of the order of 1-2%.

The formalism of the eikonal approximation is briefly given in sect. 2. In sect. 3, the calculated reaction cross-sections in nucleon-induced reactions with ^{9}Be and ^{12}C targets are presented. We discuss the sensitivity of the results to the nucleon-target interaction potential, and, in particular, the structure of the ^{9}Be target nucleus. The results of the calculations are compared with available experimental data. Section 4 is devoted to the analysis of the deuteron breakup and reaction cross-sections. Conclusions are given in sect. 5.

2 Formalism

In the eikonal approximation [5,29], cross-sections are determined by the initial WF of a projectile and profile functions describing the interaction of the projectile fragments with a target. The initial WF of the projectile $\Psi_{l_0m_0}(\mathbf{r})$ is the intrinsic WF of the relative motion of the core and valence nucleon with angular momentum l_0 and its projection m_0. It depends on the relative coordinate $\mathbf{r}$ between the nucleon and the core. In the case of the deuteron projectile, the core and valence particle refer to the neutron and proton, respectively.

After interaction with a target, the projectile intrinsic WF has the form [5]

$$\Psi(\mathbf{r},\mathbf{R}) = S_n(|\mathbf{b}_n|)S_p(|\mathbf{b}_p|)\Psi_{l_0m_0}(\mathbf{r}), \qquad (2)$$

where $\mathbf{R}$ is the coordinate of the center of mass of the deuteron, and $\mathbf{b}_n$ and $\mathbf{b}_p$ are the transverse two dimensional impact parameters of the neutron and the proton with respect to the target nucleus, *i.e.* $\mathbf{b}_n = \mathbf{R}_\perp - \frac{1}{2}\mathbf{r}_\perp$ and $\mathbf{b}_p = \mathbf{R}_\perp + \frac{1}{2}\mathbf{r}_\perp$, where $\mathbf{R}_\perp$ and $\mathbf{r}_\perp$ are the tangential components of $\mathbf{R}$ and $\mathbf{r}$ (z-axis coincides with beam direction). The profile functions $S_n(|\mathbf{b}_n|)$ and $S_p(|\mathbf{b}_p|)$ are generated by the neutron and proton interactions with the target nucleus. The profile functions S_ν ($\nu = p,n$) are determined by the integrals

$$S_i(b_i) = \exp\left[-\frac{i}{\hbar v}\int\limits_{-\infty}^{\infty} \mathrm{d}z\ V_{\nu T}\left(\sqrt{b_\nu^2+z^2}\right)\right], \qquad (3)$$

where $V_{\nu T}(r)$ ($\nu = p,n$) is the nucleon-target interaction potential and v is the beam velocity in the laboratory system.

The deuteron WF and the profile functions, determine various cross-sections of the deuteron-target interaction. The cross-sections of nucleon stripping $\sigma^{\nu}_{\rm str}$ ($\nu = n,p$), diffraction breakup $\sigma_{\rm dif}$, and deuteron absorption $\sigma_{\rm abs}$ are given by the following equations (see, for example [5,4]):

$$\begin{aligned}
\sigma^{p}_{\rm str} &= \frac{1}{2l_0+1}\sum_{m_0}\int \mathrm{d}^2\mathbf{R}_\perp \int \mathrm{d}^3\mathbf{r}\,|\Psi_{l_0m_0}|^2\,(1-|S_p|^2)|S_n|^2,\\
\sigma^{n}_{\rm str} &= \frac{1}{2l_0+1}\sum_{m_0}\int \mathrm{d}^2\mathbf{R}_\perp \int \mathrm{d}^3\mathbf{r}\,|\Psi_{l_0m_0}|^2\,(1-|S_n|^2)|S_p|^2,\\
\sigma_{\rm dif} &= \frac{1}{2l_0+1}\sum_{m_0}\int \mathrm{d}^2\mathbf{R}_\perp \left[\int \mathrm{d}^3\mathbf{r}\,|\Psi_{l_0m_0}|^2\,|S_nS_p|^2\right.\\
&\quad \left.-\sum_m\left|\int \mathrm{d}^3\mathbf{r}\,\Psi^*_{l_0m}\,S_nS_p\,\Psi_{l_0m_0}\right|^2\right],\\
\sigma_{\rm abs} &= \frac{1}{2l_0+1}\sum_{m_0}\int \mathrm{d}^2\mathbf{R}_\perp \int \mathrm{d}^3\mathbf{r}\ |\Psi_{l_0m_0}|^2\\
&\quad \times(1-|S_p|^2)\,(1-|S_n|^2). \qquad (4)
\end{aligned}$$

The deuteron-nucleus reaction cross-section is given by

$$\begin{aligned}
\sigma^{D}_{R} &= \frac{1}{2l_0+1}\sum_{m_0}\int \mathrm{d}^2\mathbf{R}_\perp\\
&\quad \times\left[1-\sum_m\left|\int \mathrm{d}^3\,\mathbf{r}\,\Psi^*_{l_0m}(\mathbf{r})\,S_nS_C\,\Psi_{l_0m_0}(\mathbf{r})\right|^2\right]. \qquad (5)
\end{aligned}$$

The reaction cross-section of the deuteron-nucleus interaction is determined by the sum of the deuteron breakup and deuteron absorption cross-sections

$$\sigma^{D}_{R} = \sigma^{n}_{\rm str} + \sigma^{p}_{\rm str} + \sigma_{\rm abs} + \sigma_{\rm dif}\,. \qquad (6)$$

The nucleon removal cross-section $\sigma_{-\nu}$ is

$$\sigma_{-\nu} = \sigma^{\nu}_{\rm str} + \sigma_{\rm dif}\,, \qquad \nu = p,n. \qquad (7)$$

The evaluation of the profile functions in the expressions for the cross-sections (4), requires a potential model for interaction between the target nucleus and the constituents of the deuteron (different representations of profile functions can be found in the literature [4–6,29–32]).

To calculate the nucleon-target interaction potential $V_{\nu T}(r)$ in (3) at incident energies less than 200 MeV we use two sets of the parameters of the global nucleon-nucleus optical potential. For the calculations at energies $10 < E_p < 65$ MeV (OP1), the parameters are taken from ref. [24]. In the case of energies $80 < E_p < 180$ MeV, the parameters (OP2) from ref. [25] are used.

For calculations of $V_{\nu T}(r)$ at the energy range from 40 to 2000 MeV, we use also the interaction potentials $V^{NN}_{\nu T}$ generated from free NN interaction cross-sections [26,27]. The parameters of the NN cross-sections are suggested in ref. [26] for incident energies from 20 to 2000 MeV. However, the most reliable results are obtained at high incident

energies, where many-body effects are small, and the free nucleon-nucleon cross-sections can be used. For energies of less than 180 MeV, we can compare the results of the calculations of the cross-sections obtained with different interaction potentials (OP1, OP2 or the potential $V_{\nu T}^{NN}$ generated from the NN interaction cross-sections).

The nucleon-target interaction potential is calculated from the NN cross-sections, assuming that the potential is proportional to the density of the target (the finite range of the NN interaction is ignored) [5]

$$V_{\nu T}^{NN}(r) = -\frac{i}{2}\hbar v\ \rho_T(r)(\tilde{\sigma}_{nn}(N_T N_\nu + Z_T Z_\nu) + \tilde{\sigma}_{np}(N_T Z_\nu + Z_T N_\nu)), \quad (8)$$

N_ν and Z_ν ($\nu = n, p$) are $N_n = 1$, $Z_n = 0$ for neutron and $N_p = 0$, $Z_p = 1$ for proton, N_T and Z_T are the number of neutrons and protons for the target nucleus. The matter distribution of the target is given by the one-particle density ρ_T. In eq. (8), $\tilde{\sigma}_{nn} = \sigma_{nn}(1 - i\alpha_{nn})$ and $\tilde{\sigma}_{np} = \sigma_{np}(1 - i\alpha_{np})$ (it is assumed that $\tilde{\sigma}_{nn} = \tilde{\sigma}_{pp}$, and $\tilde{\sigma}_{pn} = \tilde{\sigma}_{np}$), where σ_{nn} and σ_{np} are the individual NN total cross-sections, which are known with the accuracy ±1–4% over the energy range from 100 to 2200 MeV [27]. In the calculations we use tabulated σ_{nn}, σ_{np} and α_{nn}, α_{np} from ref. [27], given at different energies. To estimate the cross-sections σ_{nn} and σ_{np} at an arbitrary energy, we use the parametrization from ref. [26].

3 Nucleon-target profile functions

The profile functions $S_\nu(|\mathbf{b}|)$ enter the expression for the nucleon-target reaction cross-section

$$\sigma_R^\nu = \int \mathrm{d}\mathbf{b}\,(1 - |S_\nu(|\mathbf{b}|)|^2)\,. \quad (9)$$

Thus, the comparison of the calculated reaction cross-sections with experimental data provides a test of the profile functions $S_\nu(|\mathbf{b}|)$ ($\nu = n, p$) in the expressions for the deuteron breakup cross-sections (4) and the deuteron reaction cross-sections (5).

The profile functions $S_\nu(|\mathbf{b}|)$ are defined by the nucleon-target interaction potential (3), which can be obtained with the global nucleon-nucleus optical potential or the NN interaction cross-sections. In the case of calculations with the optical potentials OP1 and OP2, we have no free parameters in the profile functions. In the case of the calculations with the interaction potential $V_{\nu T}^{NN}$ (8), a free parameter is the density distribution $\rho_T(r)$ of the target nucleus.

As a first step in our investigation, we analyze the sensitivity of the cross-sections to the nucleon-target interaction potentials and, in particular, the density distribution of the target nucleus $\rho_T(r)$.

Since in the case of reactions with light targets at intermediate and high energies, the role of the Coulomb interactions is small (see, for example [14,28]), the sensitivity of the cross-sections to variations of the nucleon-target interaction potential is illustrated by an example of the proton-induced reaction cross-sections.

In the case of the ^{12}C target, the density distribution of the stable, tightly bound spherical nucleus ^{12}C is well investigated [33]. There are also extensive experimental data on nucleon-nucleus and deuteron-nucleus reaction cross-sections in a wide incident energy range. Most of optical model parameters (OP1, OP2) and $V_{\nu T}^{NN}$ interaction parameters are fitted to the data for tightly bound spherical nuclei and reproduce well the cross-sections.

In contrast to carbon, the ^{9}Be nucleus is expected to have a more complicated spatial structure, caused by the weakly bound (1.66 MeV) p-wave neutron. We can simulate the density distribution, assuming ^{9}Be to be a structureless nucleus, or a complex system (^{8}Be + n).

In the first case, the target density distribution ρ_{TH} is obtained for ^{9}Be with the harmonic oscillator model [33] and parametrized as

$$\rho_{TH}(x) = \rho_{0H}[1 + \alpha(x/a)^2]\exp(-(x/a)^2). \quad (10)$$

This expression contains one free parameter a. The parameter α is related to a [33]. The parameter a is fitted to reproduce the root mean square radius of the charge distribution of the target nucleus $\langle r_{\rm ch}^2\rangle^{1/2}$, related to the r.m.s. radius as $\langle r_{\rm ch}^2\rangle = \langle r^2\rangle + (0.8)^2$. The density ρ_{TH} is normalized to unity, and ρ_{0H} is a normalization factor.

The density distribution of the complex system (^{8}Be+n), ρ_{TC}, is generated from the WF of the $^8\mathrm{Be} - n$ relative motion. The density of the target is expressed as the folding of the ^{8}Be density (10) and the WF of the p-wave valence neutron $R_{l=1}(r)$

$$\rho_{TC}(r) = \rho_{0C}\left\{R_{l=1}^2\left(\frac{9}{8}r\right) + 8\int \mathrm{d}^3\mathbf{x}\rho_{TH}^{^8\mathrm{Be}}\left(\left|\mathbf{r} - \frac{1}{9}\mathbf{x}\right|\right)R_{l=1}^2(x)\right\} \quad (11)$$

and normalized to unity. This expression is obtained in the assumption of point-like nucleons. The parameters of the ^{8}Be density distribution $\rho_{TH}^{^8\mathrm{Be}}$ are fitted to reproduce the mean charge radius of ^{9}Be, which is $\langle r_{\rm ch}^2\rangle^{1/2} = 2.512$ fm [33], calculated with the WF of the $^8\mathrm{Be} - n$ relative motion. They are found to be $a = 1.659$ fm and $\alpha = 0.577$.

The WF of the $^8\mathrm{Be} - n$ relative motion is a solution of the Schrödinger equation for the Woods-Saxon potential with the parameters $V_0 = -45.54$ MeV, $R_0 = 2.4$ fm, $a_0 = 0.5$ fm.

Both distributions ρ_{TC} and ρ_{TH} reproduce the r.m.s. charge radius of ^{9}Be (2.512 fm) and the difference between them is not very essential. The density ρ_{TC} determined in (11) differs from ρ_{TH} (10) by a long tail at large distances, due to the extended distribution of the weakly bound p-wave neutron. The nucleon-target reaction cross-sections (9) calculated with ρ_{TC} (11) are larger then those obtained with ρ_{TH} (10) (fig. 1a)) by 3%.

In fig. 1, the reaction cross-sections for nucleon-induced reactions on ^{9}Be and ^{12}C targets calculated with the target densities ρ_{TH} (10) and ρ_{TC} (11) (fig. 1a)) are

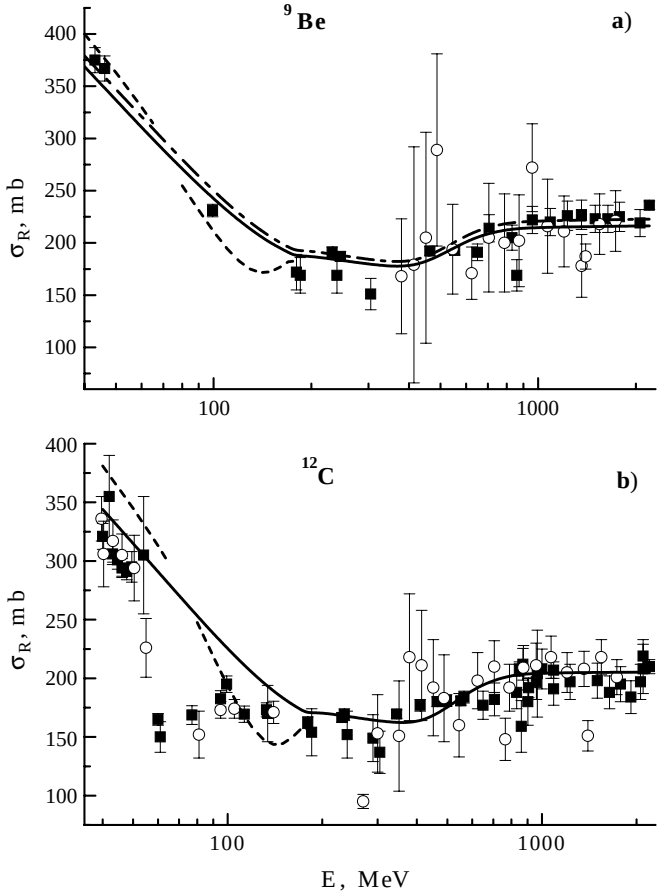

Fig. 1. The nucleon-target reaction cross-sections for a) ^{9}Be and b) ^{12}C targets. Solid lines are the calculations with the $V_{\nu T}^{NN}$ interaction potential and the target density distribution ρ_{TH}. Dashed lines correspond to calculations with the optical model potentials. Dash-dotted line in a) corresponds to the calculations with $V_{\nu T}^{NN}$ potential and the target density distribution ρ_{TC}. Squares and circles are the experimental data for the proton- and neutron-induced reactions from the compilation [18], respectively.

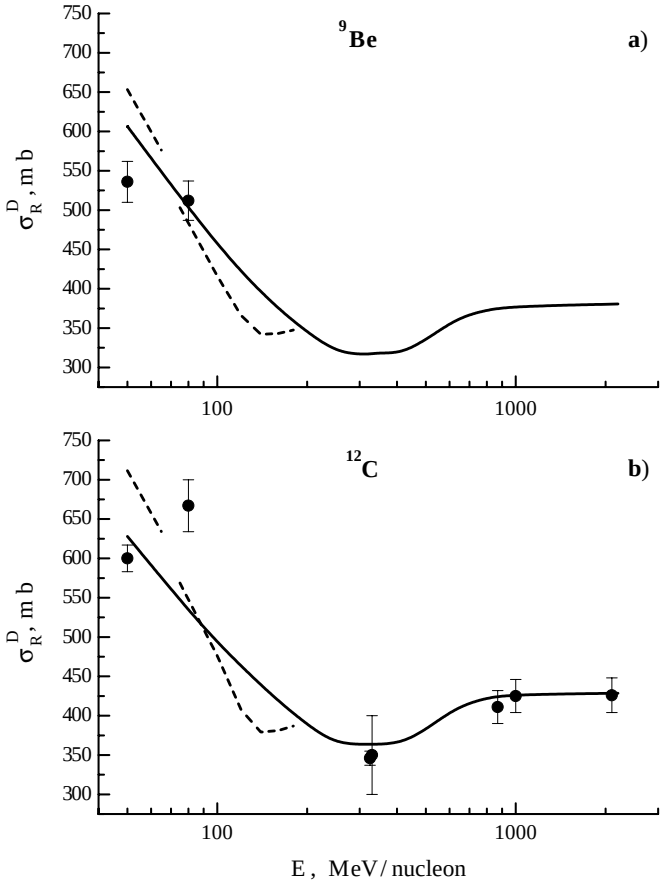

Fig. 2. The deuteron-nucleus reaction cross-sections for a) ^{9}Be and b) ^{12}C target nuclei. Solid curves are obtained with the $V_{\nu T}^{NN}$ interaction potential and dashed curves are obtained with the optical model potentials. Circles represent the experimental data from [18–23].

shown by solid and dash-dotted lines, respectively. The squares and circles correspond to the experimental data for the proton- and neutron-induced reactions [18].

As revealed by our calculations, the more complex spatial distribution, ρ_{TC}, of the ^{9}Be target leads to an increase in the proton removal cross-section $\sigma_{-\nu}$, the neutron stripping cross-section $\sigma_{\rm str}^{\nu}$, the absorption cross-section $\sigma_{\rm abs}$, by 2–4%, and to a decrease in the diffraction cross-section, $\sigma_{\rm dif}$, by 3%. For all the cross-sections the variations are negligible in comparison with the experimental accuracy of the measurements of the corresponding cross-sections. For this reason, we will mainly use the density distribution of the ρ_{TC} type in our calculations.

To analyze the sensitivity of the reaction cross-sections and the breakup cross-sections to the nucleon-target interaction potential, the cross-sections calculated with the $V_{\nu T}^{NN}$ interaction potential [26] (solid lines in fig. 1 and fig. 2) and the optical model interaction potentials $V_{\nu T}(r)$ (OP1, OP2) are compared. In fig. 1 and fig. 2, the proton reaction cross-sections obtained with the optical nucleon-nucleus potentials [24,25] are given by the dashed lines. For both C and Be targets the use of different potentials at energies near 120 MeV leads to changes of the reaction cross-sections of about 20%. As can be seen in fig. 1a) and 1b), we have a good agreement with experimental data [18] for the case of the $V_{\nu T}^{NN}$ interaction potential for ^{9}Be in the whole energy range and for ^{12}C at energies above 200 MeV. For the case of ^{12}C target at energies less than 200 MeV there is an overestimation of the experimental data for both the $V_{\nu T}^{NN}$ and optical model potentials. In general, all the interaction potentials reproduce well the experimental data.

Thus, at energies above 200 MeV, the estimation of the nucleon-target reaction cross-sections with our profile functions $S_\nu(|\mathbf{b}|)$ ($\nu = n, p$) is reliable to 3%, and we expect them good enough for the calculations of the deuteron reaction cross-sections and deuteron breakup cross-sections. At energies less than 200 MeV the dependence on the nucleon-target interaction potential is more pronounced. Hereafter, we give the calculated cross-sections obtained with both the $V_{\nu T}^{NN}$ interaction potential and optical model potentials OP1, OP2.

4 Study of the deuteron breakup reactions

Let us consider for a moment that the intrinsic WF is a pure s-wave. The correction for the d-wave is small and will be given later in this sections. In this case, the expressions for the cross-sections (4), (5) are simplified. Using the profile functions S_n and S_p, which have been checked above, we calculate the deuteron reaction cross-section as

$$\sigma_R^D = \int \mathrm{d}^2\mathbf{R}_\perp \left[1 - \left|\int \mathrm{d}^3\,\mathbf{r}\; S_n S_p\; |\Psi_{00}(\mathbf{r})|^2\right|^2\right].$$

In fig. 2, the deuteron reaction cross-sections are presented for a) ^{9}Be and b) ^{12}C targets. The solid curves are the cross-sections calculated with the $V_{\nu T}^{NN}$ interaction potential (8). The dashed curves correspond to the calculations with the optical nucleon-nucleus potentials. For the ^{12}C target (fig. 2b)) we have a very good agreement with the experimental data at energies above 200 MeV/nucleon and reasonable agreement at energies below 100 MeV/nucleon. In the case of a ^{9}Be target there are no experimental data at energies above 200 MeV/nucleon to compare with. At energies less than 200 MeV/nucleon the experimental data are reproduced reasonably well with both types of the nucleon-target interaction potential. Thus, in general, for both the ^{12}C and ^{9}Be targets we obtain a good agreement with available experimental data with both types of the nucleon-target interaction potential.

The difference between the deuteron reaction cross-section σ_R^D and the neutron reaction cross-section σ_R^n gives the proton removal cross-section (1). The experimental data on σ_R^D and σ_R^n have been well reproduced by our calculations at energies above 200 MeV/nucleon. Thus, we expect a good description of the experimental values of the removal cross-section with the realistic WF neutron-proton motion.

To analyze the sensitivity of the proton removal cross-section σ_{-p} to the deuteron intrinsic WF, we also perform the calculations with another WF $\Psi_{l_0 m_0}(\mathbf{r})$, reproducing the separation energy and the r.m.s. radius of the deuteron, and the WF in the Yukawa form. The first WF is obtained as a solution of the Schrödinger equation with the Gaussian potential (with the parameters $V_0 = -48.26$ MeV, $R_0 = 1.90$ fm). The Yukawa WF with the slope parameter a, defined by the separation energy, gives the deuteron r.m.s. matter radius 1.54 fm.

As was shown in [8,11,12], the cross-sections are proportional to the deuteron size. Our calculations with the different WFs verify this correlation. Thus, the underestimation of the r.m.s. radius with the Yukawa WF leads to the corresponding underestimation of the proton removal cross-section σ_{-p} by 20%, compared to the case of the realistic WF.

The difference between the breakup cross-sections, obtained with different types of the wave functions reproducing the binding energy and the deuteron radius is small (less than 3%). Thus, if the deuteron intrinsic WF reproduces the separation energy and the r.m.s. matter radius of the deuteron, the variations of the breakup cross-sections are small, compared to the accuracy of the experimental data on the cross-sections (fig. 3).

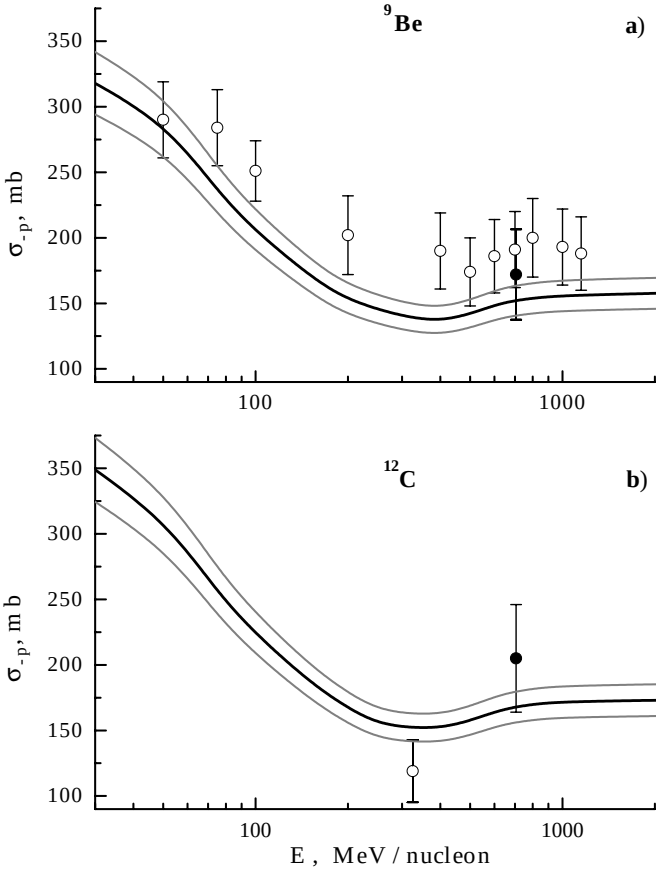

Fig. 3. The proton removal cross-section $\sigma_{-p} = \sigma_{\mathrm{str}}^p + \sigma_{\mathrm{dif}}$ in the deuteron breakup on a) ^{9}Be and b) ^{12}C target nuclei. Black curves are the results of the calculations. Empty and filled circles in a) represent the experimental data from [17] and [34]. In b) they represent the experimental data from [34] and [28]. Gray lines limit the region of possible changes of the cross-section within 7.5%.

The results of the calculations of the proton removal cross-sections σ_{-p} as functions of the deuteron energy are shown by solid lines in fig. 3.

The results of the cross-section calculations have the uncertainty, related to the more sophisticated spatial distribution of the ^{9}Be target (about 2–4%), and the uncertainty connected to the deuteron radius $R_D \simeq 2.041 \pm 0.075$ fm (the choice of the deuteron intrinsic WF) which is about $\pm$ 3.7%. If we take into account these uncertainties, the overall uncertainty of the theoretical calculations will be $\pm$ 7.5% for ^{9}Be and slightly better for ^{12}C. This accuracy is shown in fig. 3 by gray lines.

It should be also taken into account, that the deuteron ground state is an admixture of the s-wave state and the d-wave state, which is about 5% (see, for example, ref. [35]). The d-wave state contributes less to the deuteron breakup, and the admixture leads to a decrease (within 1.5%) in the proton removal cross-section.

One can see in fig. 3b), where the proton removal cross-sections are presented for a carbon target, that the results of the calculations are in a good agreement with available experimental data [28,34] at deuteron energies above 300 MeV/nucleon. It should be noted, that in the case of the ^{12}C target, we can perform a double test of results, using eq. (1) which relates the nucleon-target reaction cross-section, deuteron reaction cross-section and the proton removal cross-section at the same incident energy per nucleon. First, we can check the theoretical results shown by solid lines in fig. 1b), fig. 2b), fig. 3b) and we have found that the results are consistent. Second, we can use just experimental data at energies above 200 MeV/nucleon, shown in fig. 1b), fig. 2b), fig. 3b) for the same check. This check shows the self-consistence of the experimental cross-sections in the limits of error bars.

Comparing the results of the calculations of the proton removal cross-sections on the ^{9}Be target (fig. 3a) with the experimental data from [17,34] one can see that the theoretical curve reproduces well the energy dependence of the cross-sections. However, at energies above 200 MeV/nucleon the theoretical results underestimate the cross-section. In the case of the ^{9}Be target we have checked that theoretical cross-sections satisfy eq. (1). However, for deuteron energies above 200 MeV/nucleon the corresponding comparison with experimental data is impossible because of the lack of the experimental data for the deuteron reaction cross-sections for the ^{9}Be target (see fig. 2a)).

5 Conclusions

In our analysis of the deuteron breakup, the deuteron has been considered as a two-body halo-like nuclear system. The reaction cross-sections and proton removal cross-sections in the deuteron-induced reactions on carbon and beryllium targets have been calculated in the eikonal approximation of the Glauber model at intermediate and high energies. The sensitivity of the cross-sections to the input parameters of the eikonal approximation has been analyzed.

The results are the most sensitive to the choice of the deuteron intrinsic wave function at the deuteron energies above 200 MeV/nucleon, while at lower energies, the results are also sensitive to the choice of the nucleon-target interaction potential.

Thus, one can expect that the eikonal approximation is a good approach for studies on one-nucleon removal cross-sections in the reactions with exotic nuclei at intermediate and high energies as far as the information about the target and the core fragments and the nucleon-target interaction potential is reliable.

The results of calculations for the deuteron-induced reactions show a good agreement with experimental data for a carbon target [18–23]. However, for this target essentially more experimental data for proton removal cross-sections in the energy range from 200–2000 MeV/nucleon are needed for realistic estimations of the accuracy of the model.

For the beryllium target, the calculations reproduce well the energy behavior of the experimental proton removal cross-sections measured recently [17]. It should be noted that, in this case, the theoretical calculations systematically underestimate the measured cross-sections at energies above 200 MeV/nucleon. To get an answer about this discrepancy it is necessary to have experimental data on the deuteron reaction cross-sections in the same energy range, which are not available now.

Since eikonal approximation of the Glauber model is widely used now for studies on exotic (halo) nuclei, and the deuteron is one of the best candidate for a test of this model, it seems very important to have additional experimental data for deuteron-induced reactions on light targets.

References

1. G.F. Bertch, K. Hencken, H. Esbensen, Phys. Rev. C **57**, 1366 (1998).
2. H. Esbensen, K. Hencken, Phys. Rev. C **61**, 054606 (2000).
3. D. Ridikas, M.H. Smedberg, J.S. Vaagen, M.V. Zhukov, Nucl. Phys. A **628**, 363 (1998).
4. Yu. L. Parfenova, M.V. Zhukov, J.S. Vaagen, Phys. Rev. C **62**, 044602 (2000).
5. K. Hencken, G. Bertsch, H. Esbensen, Phys. Rev. C **54**, 3043 (1996).
6. J.A. Tostevin, J. Phys. G: Nucl. Part. Phys. **25**, 735 (1999).
7. R.J. Glauber, in *Lectures on theoretical Physics*, edited by W.E. Brittin, L.C. Dunham, Vol. **1** (Interscience, New York, 1959) p. 315.
8. R.J. Glauber, Phys. Rev. **99**, 1515 (1955).
9. C.A. Bertulani, K.W. McVoy, Phys. Rev. C **46**, 2638 (1992).
10. Y.A. Berezhnoy, V.Y. Korda, Nucl. Phys. A **556**, 453 (1993).
11. R. Serber, Phys. Rev. **72**, 1008 (1947).
12. A.I. Akhieser, A.G. Sitenko, Phys. Rev. **106**, 1236 (1957).
13. E.L. Feinberg, Zh. Eksp. Teor. Fiz. **29**, 115 (1955) (Sov. Phys. JETP **2**, 58 (1956)).
14. G. Fäldt, Phys. Rev. D **2**, 846 (1970).
15. J.C. Peng, R.M. DeVries, N.J. DiGiacomo *et al.*, Phys. Lett. B **98**, 244 (1981).
16. F. Carstoiu, C. Lazard, R.J. Lombard, Phys. Rev. C **57**, 2638 (1998).
17. J.F. Lecolley, C. Varignon, J. Thun *et al.*, Eur. Phys. J. A **5**, 321 (1999).
18. V.S. Barashenkov, *Secheniya vzaimodeistviya chastits i yader s yadrami* (JINR, Dubna, 1993).
19. A. Auche, R.F. Carlson, A.J. Cox *et al*, Phys. Rev. C **53**, 2919 (1996).
20. P. Millburn, W. Birnbaum, W.F. Grandall *et al.*, Phys. Rev. **95**, 1269 (1954).
21. V.V. Avdeichikov, G.G. Beznogih, V.A. Budilov *et al.*, Yad. Fiz. **30**, 610 (1979).
22. H. de Vries, C.W. de Jager, C. de Vries, Phys. Rev. Lett. **43**, 1373 (1979).
23. J. Jaros, A. Wagner, L. Anderson *et al.*, Phys. Rev. C **18**, 2273 (1978).
24. R.L. Varner, W.J. Thompson, T.L. Mcabee *et al.*, Phys. Rep. **201**, 57 (1991).

25. A. Nadasen, P. Schwandt, P.P. Singh *et al.*, Phys. Rev. C **23**, 1023 (1981).
26. S.K. Charagi, S.K. Gupta, Phys. Rev. C **41**, 1610 (1990).
27. L. Ray, Phys. Rev. C **20**, 1857 (1979).
28. J.D. Jafar *et al.*, Nucl. Phys. A **161**, 105 (1971).
29. H. Esbensen, G.F. Bertch, Phys. Rev. C **59**, 3240 (1999).
30. A. Bonaccorso, F. Carstoiu, Phys. Rev. C **61**, 034605 (2000).
31. H. Esbensen, Phys. Rev. C **53**, 2007 (1996).
32. A. Abu-Ibrahim, K. Fujimura, Y. Suzuki, Nucl. Phys. A **657**, 391 (1999).
33. H. de Vries, C.W. de Jager, C. de Vries, At. Data Nucl. Data Tables **36**, 495 (1987).
34. G. Bizard, F. Bonthonneau, J.L. Laville *et al.*, Nucl. Instrum. Methods Sci. Res. **111**, 445 (1973).
35. R. Machleidt, Phys. Rev. C **63**, 0024001 (2001).